The astrochemical factory: A solid base for interstellar reactions

Ligterink, N.F.W.

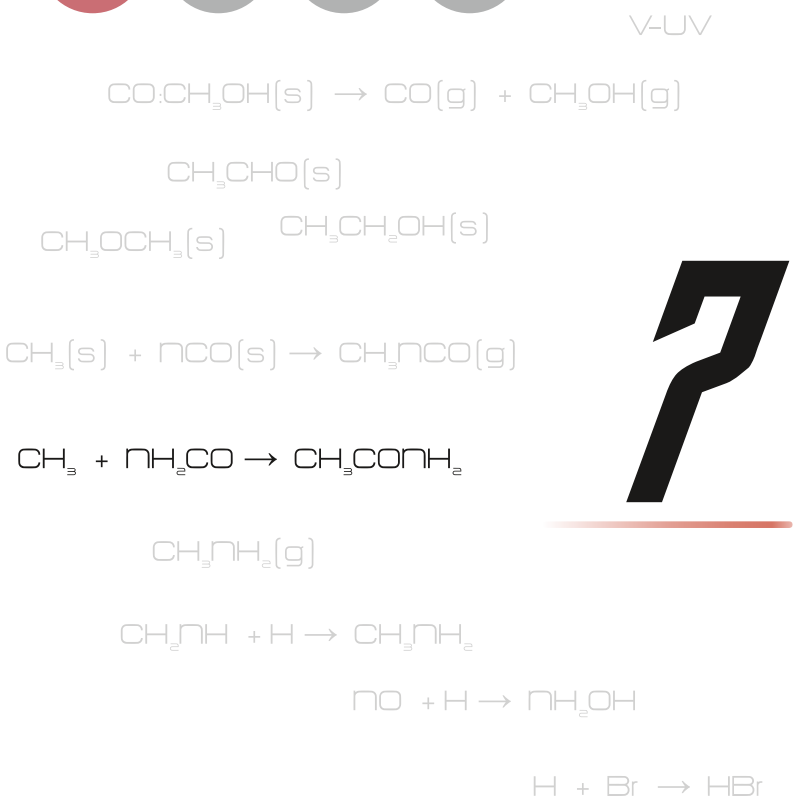

7

Formation of amides in interstellar relevant ices

N.F.W. Ligterink, J. Terwisscha van Scheltinga, E.F. van Dishoeck & H. Linnartz

Ligterink et al. 2017, in prep.

7.1. Introduction

Prebiotic molecules resemble functional groups of biotic molecules and are thought to be involved in the formation of life-bearing molecules, such as amino acids, nuclides and sugars (Herbst & van Dishoeck 2009; Caselli & Ceccarelli 2012). The interstellar presence of prebiotic molecules supports the idea that the building blocks of life may have an extraterrestrial origin. A number of prebiotic molecules have been detected in the ISM, such as the simplest sugar glycolaldehyde (Hollis et al. 2004; Jørgensen et al. 2012; Jørgensen et al. 2016) and methylamine and aminoacetonitril, potential precursors of the amino acid glycine (Kaifu et al. 1974; Belloche et al. 2008). Among prebiotics, molecules with an amide or amide-like (i.e. species that resemble the structure of an amide bond, hereafter generally also called amides) structure are of particular interest because they resemble the peptide bond that binds amino acids, see Fig 7.1. In terrestrial biochemistry amino acids link to form so-called peptide chains that eventually form proteins, the engines of life.

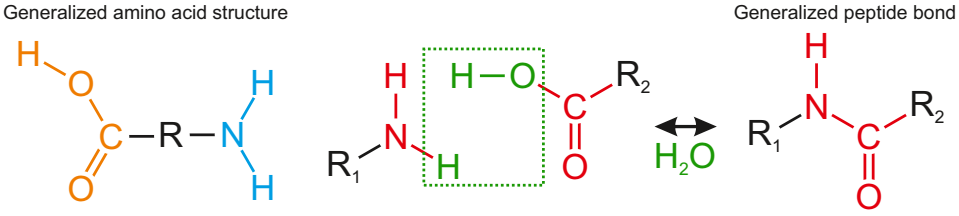

Figure 7.1: Left: General structure of an amino acid, with the acid group in orange and amine group in blue. Center: Binding between an amine and acid group while losing a water molecule. Right: Generalized peptide bonded or amide structure.

Besides being prebiotic molecules, amides are also interesting as tracers of interstellar environments due to their widespread presence throughout the ISM. Isocyanic acid (HNCO) and formamide (NH_2CHO) are the most abundant ones and have been detected in a large variety of interstellar sources (e.g., Bisschop et al. 2007b; Kahane et al. 2013; Adande et al. 2013; Corby et al. 2015; Bergner et al. 2017) and comets, including 67P/Churyumov-Gerasimenko (67P/C-G) (Bockelée-Morvan et al. 2000; Goesmann et al. 2015). Strong observational evidence exists for a formational relationship between HNCO and NH_2CHO in interstellar ice (Bisschop et al. 2007b; López-Sepulcre et al. 2015; Coutens et al. 2016). In the form of the OCN^- anion, HNCO has directly been detected in interstellar ices at abundances as high as 2% with respect to water (Lacy et al. 1984; Gibb et al. 2004; van Broekhuizen et al. 2005). Tentatively, the presence of formamide in interstellar ice has been claimed toward NGC 7538 IRS9 (Raunier et al. 2004).

The more complex molecule acetamide (CH_3CONH_2) has been detected toward Sgr B2 and Orion KL (Hollis et al. 2006; Halfen et al. 2011; Cernicharo et al. 2016; Belloche et al. 2017) and in 67P/C-G (Goesmann et al. 2015; Altwegg et al. 2017). Its formation has been be linked with the presence of formamide. Methyl isocyanate (CH_3NCO) has been detected toward Sgr B2 and Orion KL

(Halfen et al. 2015; Cernicharo et al. 2016) and recently also toward the sun-like protostar IRAS 16293–2422 (Ligterink et al. 2017; Martín-Doménech et al. 2017). Its formational origin is likely found in interstellar ices and involves reactions between (H)NCO and CH_3 radicals. Hydrogenation of CH_3NCO can lead to N-methyl formamide (CH_3NHCHO), a molecule that has tentatively been identified toward Sgr B2 (Belloche et al. 2017). Finally, carbamide, also known as urea (NH_2CONH_2), has been tentatively identified toward Sgr B2 (Remijan et al. 2014).

The high interstellar abundances of HNCO and NH_2CHO have resulted in many laboratory studies with the aim to understand their formation paths (Hagen et al. 1979; Gerakines et al. 2004; Raunier et al. 2004; Jones et al. 2011; Islam et al. 2014; Muñoz Caro et al. 2014; Fedoseev et al. 2015b, 2016; Kaňuchová et al. 2016). In these studies, ice mixtures containing a source of carbon, like CH_3OH or CO, and a source of nitrogen, such as HCN, HNCO, NH_3, N_2 or NO are hydrogenated and/or energetically processed. A number of mechnisms have been shown to produce these species, such as the NH + CO reaction to produce HNCO (Fedoseev et al. 2015b), NH_2 + CHO radical combination to produce NH_2CHO (Jones et al. 2011) and hot, i.e., energetic H-atom addition to HNCO can explain the formation of NH_2CHO (Raunier et al. 2004).

The larger amides urea and acetamide have been detected in various experiments (e.g., Berger 1961; Agarwal et al. 1985; Bernstein et al. 1995; Raunier et al. 2004; Henderson & Gudipati 2015; Förstel et al. 2016), but formation mechanisms have not been experimentally investigated. Some reactions have been proposed, such as the NH_2 + NH_2CO radical addition to form NH_2CONH_2 (Agarwal et al. 1985). Modelling investigations have predicted the formation of CH_3CONH_2 through the CH_3 + HNCO reaction followed by hydrogenation (Garrod et al. 2008) or the hydrogen abstraction of NH_2CHO followed by CH_3 addition (Belloche et al. 2017). The formation of N-methylformamide has been claimed in VUV irradiated CH_3NH_2:CO ice mixtures through the reaction CH_3NH + CHO (Bossa et al. 2012), while modelling investigations have shown that hydrogenation of CH_3NCO is one of the main channels of CH_3NHCHO formation (Belloche et al. 2017). Recently, the reaction CH_3 + (H)NCO was shown to result in the formation of CH_3NCO (Ligterink et al. 2017), a process that likely in a similar way takes places on interstellar dust grains.

In this work we aim to elucidate the chemical network that links various small amides that have been detected in the ISM and to explain their formation. This work is linked to that of Ligterink et al. (2017) and investigates reactions that can occur simultaneously with the formation of CH_3NCO. The possible hydrogen atom addition reaction $CH_3NCO + H \rightarrow CH_3NHCHO$ is one that needs further investigation. Two types of hydrogen addition can occur. With so-called hot H-atom addition the hydrogen atoms are produced in an energetic dissociation process, for example VUV induced photodissociation, and carry excess energy which allows these atoms to more easily overcome energy barriers. Hydrogenation is the term used for cold or low energy hydrogen atom addition. These atoms are usually made with hydrogen dosing beams (e.g., Fuchs et al. 2009), but can also occur when hydrogen atoms produced in energetic processes are thermalised by their surroundings. Also the radical addition reactions CH_3 + $NHCHO \rightarrow CH_3NHCHO$ and $CH_3 + NH_2CO \rightarrow CH_3CONH_2$ are possible. To

this extend mixtures of HNCO:CH_4 are VUV irradiated in order to form the CH_3 radical from methane and various intermediate radicals and products of HNCO. HNCO in the form of OCN^- and CH_4 are known to be present in interstellar ices with median abundances of 0.6 and 4.5 % with respect to water, respectively (Boogert et al. 2015). The resulting products from reactions between the two are identified and analysed.

Section 7.2 discusses the laboratory set-up and protocol. The results of the experiments are presented in Sec. 7.3 and discussed in Sec. 7.4. The conclusions of this work are presented in Sec. 7.5.

7.2. Experimental

7.2.1. Setup and protocol

For this study the CryoPAD2 setup is used, which has been described in Ligterink et al. (2017). In short it consists of a central chamber at ultra-high vacuum conditions ($P \leq 10^{-10}$ mbar). A cryogenically cooled gold-coated reflective surface is positioned at the center of the chamber. On this surface gases are deposited by direct deposition to form an ice layer, simulating the interstellar icy dust grain environment. The output of a Microwave Discharge Hydrogen-flow Lamp (MDHL, Ligterink et al. 2015, and references therein) is directed at the surface and used to energetically process the ice. Chemical changes within the ice are traced by Reflection Absorption IR Spectroscopy (RAIRS) and mass spectrometry in combination with Temperature Programmed Desorption (TPD).

MDHLs generally have strong emission at the Lyman-α transition at 121.6 nm and H_2 continuum emission between 140-160 nm. In this work we make use of lamp conditions optimized for Lyman-α rich or poor emission to process the ice samples, see Fig. 7.2, in order to test the influence of high energetic Lyman-α radiation on the chemistry in the ice. This can for example influence the production of CH_3 radicals from CH_4 as can be derived from the methane photo absorption cross section, which is high around the Lyman-α transition, but low for wavelengths longer than 140 nm (Cruz-Diaz et al. 2014b). The total photon flux is $(1.1\pm0.1)\times10^{14}$ photons s^{-1} for the Lyman-α rich emission, while it is $(6.1\pm1.0)\times10^{13}$ photons s^{-1} in the Lyman-α poor case.

Gases used during the experiments are CH_4 (Linde Gas, 99.995% purity), $^{13}CH_4$ (Sigma-Aldrich, 99% purity) and CO (Linde Gas, 99.995% purity). The regular methane gas contains the natural isotope abundances of $^{12/13}C$ of $\sim$90. However, throughout this chapter methane gas will generally be called $^{12}CH_4$ to stress the mass difference in those experiments making use of either ^{12}C or ^{13}C rich gas. Gas-phase HNCO is produced from thermal decomposition of cyuranic acid (Sigma-Aldrich, 98% purity), the solid trimer of HNCO, similar to the protocol used by van Broekhuizen et al. (2004). Freeze-pump-thaw cycles are used to purify the HNCO sample and mainly remove CO_2, O_2 and N_2. Hydrogen cyanide (HCN) impurities are sometimes present in the prepared gas, but can not be removed by this technique. Samples of solid acetamide (Sigma-Aldrich, 99% purity) and liquid N-methyl formamide (Sigma-Aldrich, 99% purity) are used for verification experiments.

Gas mixtures are prepared in a gas mixing line by volume mixing with an

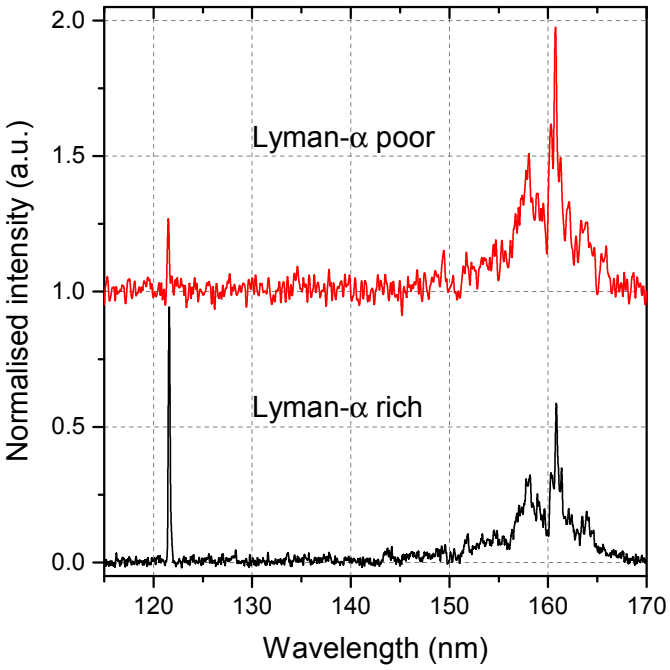

Figure 7.2: Vacuum-UV spectrum of the MDHL emission between 115 and 170 nm. The top spectrum (red) shows lamp emission poor in Lyman-α, while the bottom spectrum (black) shows lamp emission rich in Lyman-α.

gas independent gauge. The mixture is deposited on the gold-coated substrate at 20 K. Residual gases of the deposition are removed from the chamber during a short waiting period until a pressure of $\sim 1 \times 10^{-10}$ mbar is reached. Next, the samples are VUV irradiated for 20 minutes, corresponding with a total fluences of 1.3×10^{17} or 7.3×10^{16} photons for the Lyman-α rich and poor case, respectively. After irradiation the sample is heated from 20 to 300 K and the desorbing contents are analysed with a sensitive Quadrupole Mass Spectrometer (QMS) over a large range of masses. After deposition and during irradiation and TPD, IR spectra are recorded at 1-2 cm^{-1} resolution using a Fourier Transform InfraRed Spectrometer (FTIRS, 500-4000 cm^{-1}) to trace chemical changes in the ice.

7.2.2. Data analysis

IR data

RAIR spectra of the experiments are baseline subtracted and IR features are identified by comparing with literature data. Deviations between literature values and this work can arise from differences in transmission versus reflection

Table 7.1: Peak positions and transmission bandstrengths of parent and product species

Species	band	Peak position (cm^{-1})		Band strength cm $molecule^{-1}$
		Literature	Experiment*	
$HNCO^{a}$	OCN str.	2260	2266	7.8×10^{-17}
CH_4 [b]	d-str.	1301	1302	7.3×10^{-18}
CH_4 [b]	d-str.	3010	3010	1.1×10^{-17}
CO^{c}	CO str.	2138	2142	1.1×10^{-17}
$OCN^{-,a}$	OCN str.	2160	2170	1.3×10^{-16}
CO_2 [c]	CO a-str.	2342	2341	7.6×10^{-17}
$HCN^{d,**}$	CN str.	2099	2108	–
$CH_3NCO^{e,**}$	NCO a-str.	2322	2322	–
CH_3CH_3 [f]	CH_3 d-str.	2975	2976	6.5×10^{-18}
$NH_4^{+,a}$	deform.	1485	1466	4.6×10^{-17}
$NH_2CHO^{g,h}$	CO str.	1700	∼1687	3.3×10^{-17}
NH_2CONH_2 [h]	CO str.	1590	–	–
NH_2CONH_2 [h]	NH s-bend	1675	∼1687	–
NH_2CONH_2 [h]	NH a-bend	1630	∼1687	–

Notes. *Peak positions found for experiment 1 (see Table 7.2); **Indicates IR data obtained from reflection experiments. [a]van Broekhuizen et al. (2004), water poor conditions; [b]Hudgins et al. (1993); Boogert et al. (1997); [c]Bouilloud et al. (2015); [d]Gerakines et al. (2004); [e]Ligterink et al. (2017); [f]Gerakines et al. (1996); [g]Wexler (1967); [h]Raunier et al. (2004)

values or matrix effects. The column density (N_{species}) of an IR feature is determined from its integrated band area ($\int_{\text{band}} \tau d\nu$) by:

$$N_{\text{species}} = \frac{1.1}{3.4} ln(10) \frac{\int_{\text{band}} \tau d\nu}{A_{\text{band}}}, \tag{7.1}$$

where A_{band} is the bandstrength of a specific band of a species and $\frac{1.1}{3.4}$ is a RAIRS scaling factor. Due to longer pathlength through the ice and dipole surface coupling, the RAIRS sensitivity differs from transmission IR spectroscopy and therefore bandstrength values are different from transmission bandstrength values. For the CryoPAD2 setup the bandstrength of the CO stretch mode of carbon monoxide at 2138 cm^{-1} is determined to be $3.4^{+0.5}_{-0.5} \times 10^{-17}$ cm $molecule^{-1}$ (Ligterink et al. 2017, subm.). Using the transmission bandstrength of 1.1×10^{-17} cm $molecule^{-1}$ for the same CO mode (Bouilloud et al. 2015) and assuming that for identical conditions band strengths of different molecules scale in the same way, the general scaling factor between RAIRS and transmission IR spectroscopy of $\frac{1.1}{3.4}$ is found.

Table 7.1 gives an overview of band positions and bandstrength values of parent and expected product species. Most IR parameters are taken from transmission experiments available from literature, with the exception of the HCN CN stretching mode and CH_3NCO NCO asymmetric stretching mode

(Gerakines et al. 2004; Ligterink et al. 2017, respectively).

Recently methane gained interest due to inconsistencies in literature on the assignment of methane modes in amorphous or crystalline phase (Gerakines & Hudson 2015). Experiments in this work are conducted with ices at temperatures of 20 K and therefore we consider the methane to be of crystalline nature. Consequently, we choose to use a *crystalline bandstrength value* by applying the same correction as performed by Boogert et al. (1997) on data recorded by Hudgins et al. (1993) to retrieve the bandstrength for the CH_4 mode at 3010 cm^{-1} as 1.1×10^{-17} cm $molecule^{-1}$. Finally, because no water is used in these experiments, the water-poor bandstrength values listed by van Broekhuizen et al. (2004) are used for HNCO and OCN^-.

Temperature Programmed Desorption QMS data

During TPD, parent and product species desorb from the gold surface and are measured by the QMS, with an ionization source tuned to 70 eV. Each species has a characteristic desorption temperature and fragmentation pattern which can be used for identification. However, this is not always as straight forward. Species can have desorption temperatures close together or co-desorb with each other. A desorption signal at a certain m/z measured by the QMS can therefore have two or more contributions. In these experiments particularly the parent species HNCO, which desorbs around 120 K, can contaminate the TPD signal of other species. Due to its high abundance compared to reaction products, even small fragmentation channels of HNCO, such as m/z 28 and 29, can influence product fragmentation patterns. Many of the products studied in this work display similar fragmentation patterns and desorption temperatures and therefore complicate the interpretation of the TPD signal.

A number of measures are taken to circumvent some of the problems described above. First, the focus of the TPD data is on the region between 150 and 300 K, to avoid the HNCO desorption peak as much as possible. This also means that potentially co-desorbing species with HNCO are not extensively analysed. Second, isotopic labelling is used to distinguish products. Third, a specific analysis protocol is used to determine fragmentation patterns of desorbing species; The QMS output is first corrected for its work functions. For a desorption peak, all the masses that desorb at or close to the same temperature are selected. If necessary, baseline subtraction is performed to remove contributions of other desorbing species. Next, the intensity of the signal at each m/z is determined at the peak desorption temperature. These signals are normalised, mostly to the highest signal or highest m/z in the feature. The resulting fragmentation pattern is compared with literature and $in-situ$ measured fragmentation patterns of molecules.

7.2.3. Fragmentation patterns and desorption temperatures

This work relies for a large part on molecule specific desorption temperatures and mass fragmentation patterns. Desorption temperatures of many small species, like CO, water or methanol, have been well studied. However, for larger species such data are often not available. This includes two the potential isomeric products CH_3NHCHO and CH_3CONH_2. Therefore, the desorption temperatures

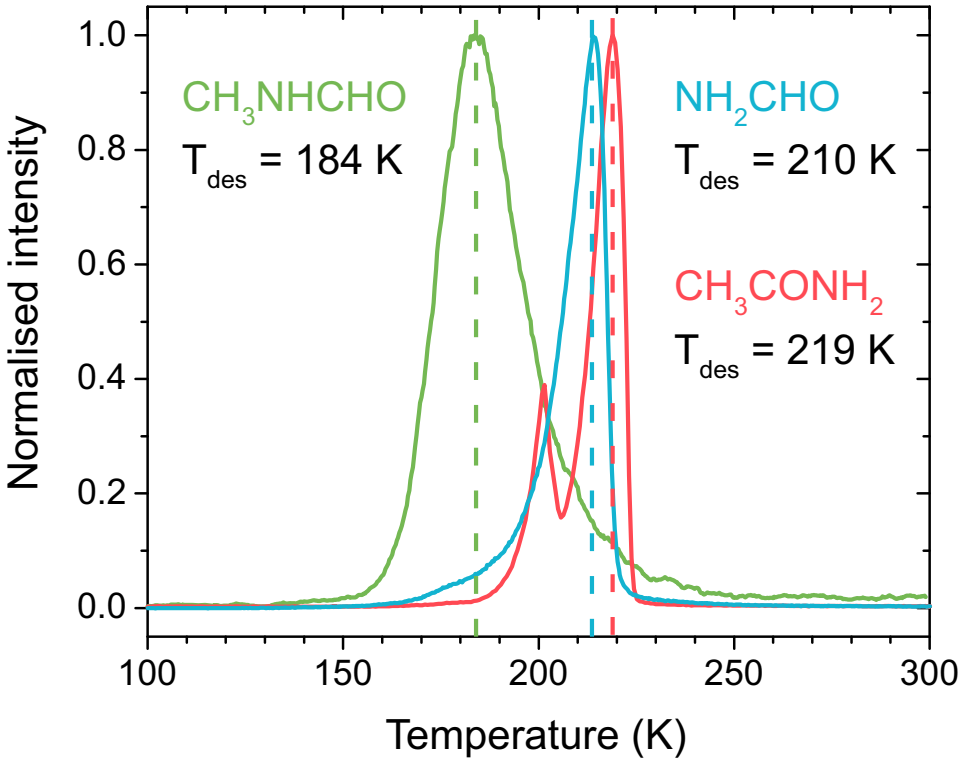

Figure 7.3: TPD traces of m/z 59 of pure N-methylformamide (green), pure formamide (blue) and pure acetamide (red).

of these two species are measured in the CryoPAD2 setup. Figure 7.3 shows the TPD traces of these two molecules at m/z 59, the main mass of both molecules. The peak desorption temperature of N-methylformamide is found at 184 K, while that of acetamide is found at 219 K. The origin of the smaller peak at ∼200 K in the acetamide TPD trace is unknown, but could be the result of acetamide desorption due to a phase change in the ice. Another important product is formamide, for which the desorption temperature is determined to be 210 K (see Fig. 7.3).

Most fragmentation patterns of parent and possible product species are available in the NIST database[1], listed for an ionization energy of 70 eV. For N-methylformamide and acetamide the NIST fragmentation patterns are compared with $in-situ$ measured fragmentation patterns, see Fig. 7.4. The general structure of both patterns is similar for each molecule. N-Methylformamide has its main fragmentation channels around m/z 30 and 29 (the CH_3NH fragment), while those of acetamide are found at m/z 44, 43 and 42 (the NH_2CO fragment). However, deviations in pattern intensities are visible, most noticeable in the m/z

[1]NIST Mass Spec Data Center, S.E. Stein, director, "Mass Spectra" in NIST Chemistry WebBook, NIST Standard Reference Database Number 69, Eds. P.J. Lindstrom and W.G. Mallard, National Institute of Standards and Technology, Gaithersburg MD, 20899, http://webbook.nist.gov.

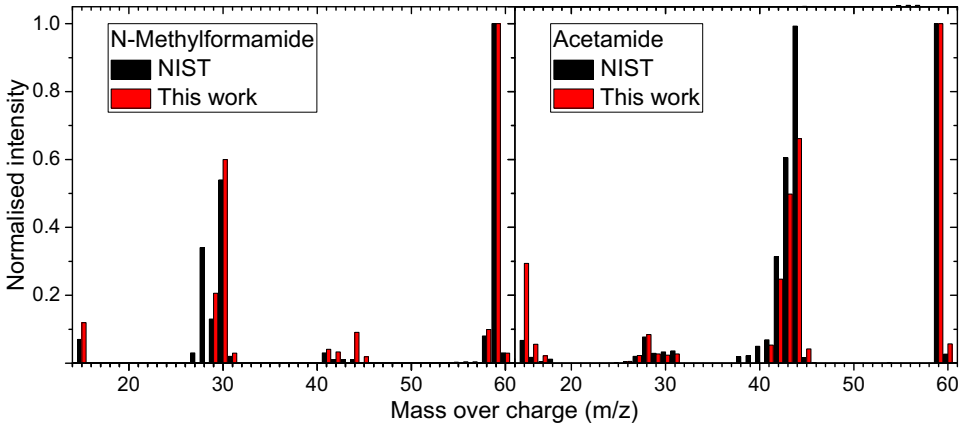

Figure 7.4: Fragmentation pattern comparison between NIST data and values measured in this work for N-methylformamide (top) and Acetamide (bottom).

44 channel of acetamide. Throughout this work the fragmentation patterns of N-methylformamide and acetamide presented here will be used. Fragmentation patterns of other species rely on NIST and literature data.

7.3. Results

7.3.1. Identification of the main products

The identification of products in the VUV processed CH_4:HNCO mixed ices is mainly based on three experiments. These are a 1:1 HNCO:$^{12}CH_4$ mixed ice, a pure HNCO ice and a 1:1 HNCO:$^{13}CH_4$ mixture. Table 7.2 lists these as (1-3) together with other experiments performed in this work. In the following subsections the IR spectroscopic data of experiment 1 and mass spectrometric data of experiment 1 to 3 are analysed.

IR analysis of VUV processed ice

Figure 7.5 shows the IR spectrum between 1200 and 3100 cm^{-1} of the HNCO:CH_4 mixture (experiment 1) before and after VUV irradiation with a fluence of 1.3×10^{17} photons. Before irradiation, besides the HNCO band at 2266 cm^{-1} and the CH_4 bands at 1302 and 3010 cm^{-1}, trace amounts of HCN and CO_2 contamination are visible at 2108 and 2341 cm^{-1}, respectively. After processing, spectroscopic features appear that can be assigned to CH_3CH_3, $OCN^-NH_4^+$ and CO. These are known products of VUV processing of pure methane and isocyanic acid ice. The presence of these products indicates that the CH_3 radical is formed and that HNCO fragments into CO and NH (or N and H separate). The NH radical reacts with H atoms or strips them from other molecules to form NH_3, which engages in an acid-base reaction with HNCO to form $OCN^-NH_4^+$.

A feature in the wing of the HNCO peak at 2322 cm^{-1} indicates the formation of CH_3NCO, as was discussed in a previous study by Ligterink et al. (2017). At

Table 7.2: Overview of performed experiments, giving deposited material at the start of the experiment and irradiation source.

Exp.	N(HNCO)	N(CH4) ML	N(CO)	Lyman-α High/Low
1	14.3	17.0	–	H
2	17.4	-	–	H
3	15.1	15.7[a]	–	H
4	29.9	5.5	–	H
5	11.4	24.6	–	L
6	2.9	8.5	95.6	L
7	4.8	13.9	164.2	L

Notes. [a]Experiment using $^{13}CH_4$, bandstrenght value of 1.1×10^{-17} is assumed to apply to the $^{13}CH_4$ degenerate stretching mode as well.

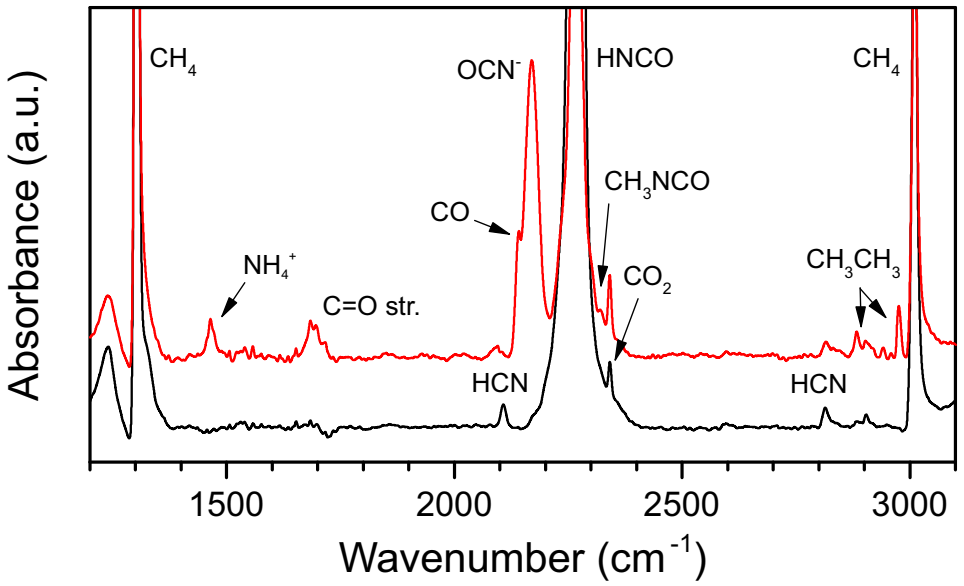

Figure 7.5: IR spectrum between 1200 and 3100 cm^{-1} before (black) and after (red) irradiation of the HNCO:$^{12}CH_4$ ice mixture of experiment 1.

$\sim$1687 cm^{-1} another feature is seen. In VUV processing of pure HNCO ice, it was identified as contributions of the H_2CO and NH_2CHO C=O stretch modes and NH bending modes of NH_2CONH_2 (Raunier et al. 2004). These species likely contribute to this feature, but can not be clearly distinguished. More complex amides, such as N-methylformamide and acetamide can contribute to this feature as well. Since other spectroscopic features characteristic of complex amides are not clearly identified in the IR spectrum, mass spectrometry must be used to identify these species. An overview of the identified peak positions in experiment 1 is given in Table 7.1.

Primary amide formation seen in TPD

Figure 7.6 shows the TPD traces between 150 and 300 K of the main masses of the simplest, or primary, amides that can be formed from HNCO:CH_4 ice mixtures. These masses are m/z 45 for NH_2CHO, m/z 59 for either CH_3CONH_2 or CH_3NHCHO and m/z 60 for NH_2CONH_2. The secondary mass channel of HNCO, m/z 42, is included as well to trace HNCO. The panels show from top to bottom the results of the $^{12}CH_4$:HNCO, HNCO and $^{13}CH_4$:HNCO experiments (experiment 1, 2 and 3, respectively).

In each of the panels a prominent trailing slope of m/z 42, with a desorption feature between 205 and 210 K is seen. The trailing slope is due to residual gas of the main HNCO desorption peak at 120 K. The desorption feature is caused by the thermal decomposition of the $OCN^-NH_4^+$ (or potentially other cations) salt complex and subsequent desorption of HNCO.

Three desorption peaks of m/z 45, 59 and 60 are visible at $\sim$207, $\sim$215 and $\sim$267 K, respectively. m/z 45 and 60 show up in all panels, including the irradiated pure HNCO ice, and are therefore photoproducts directly resulting from HNCO. Furthermore the desorption peak of m/z 45 at 207 K is close to the pure formamide desorption temperature of 210 K. This feature we identify therefore as formamide. Urea is a known product of HNCO processing (Raunier et al. 2004) and the position of the TPD trace is consistent with TPD traces of urea obtained by Förstel et al. (2016). Thus, the m/z 60 TPD trace is identified as urea.

The m/z 59 feature is caused by a reaction between CH_4 and HNCO, as can be inferred from its non-presence in the pure HNCO experiment and 1 amu mass shift to m/z 60 in the HNCO:$^{13}CH_4$ experiment. Therefore this product is either CH_3NHCHO or CH_3CONH_2. Other isomers like acetaldoxime (CH_3CHNOH) and nitrosoethane (CH_3CH_2NO) are deemed unlikely to be responsible for the m/z 59 feature, due to the many fragmentation and reaction steps that need to be invoked to form these products. The desorption peak of m/z 59 at 215 K is close to the desorption temperature of pure acetamide at 219 K. Desorption temperatures measured from pure ices are known to shift in mixed ices due to differences in binding energies of co-desorption effects. One could make the same case for N-methylformamide and claim that it is trapped in the remaining ice, mainly $OCN^-NH_4^+$ and NH_2CHO. This seems very unlikely however, due to the relatively volatile nature of CH_3NHCHO. One would expect it to desorb before or with the signal of NH_2CHO and $OCN^-NH_4^+$, which is not the case for the m/z 59 desorption feature in these TPD traces. Therefore, the m/z 59 feature is very likely the result of acetamide formation in the ice in CH_4:HNCO mixtures.

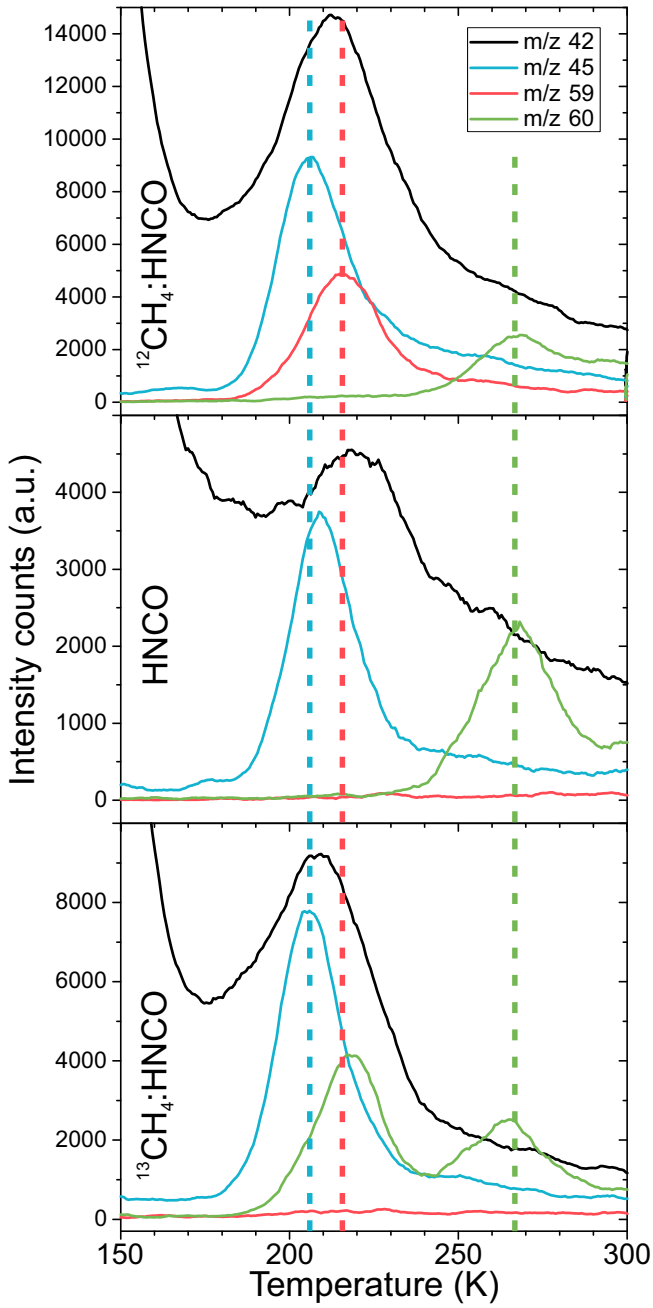

Figure 7.6: TPD traces of m/z 42 (black, HNCO), 45 (blue, NH_2CHO), 59 (red, CH_3CONH_2) and 60 (green, NH_2CONH_2) between 150 and 300 K of VUV processed HNCO:$^{12}CH_4$ (experiment 1, top), pure HNCO (experiment 2, middle) and HNCO:$^{13}CH_4$ (experiment 3, bottom) ice. Dashed lines indicate the desorption peaks of products.

Table 7.3: Mass fragmentation patterns of NH_3, HNCO, NH_2CHO and CH_3CONH_2 at selected masses.

m/z	NH_3	HNCO[a]	NH_2CHO	CH_3CONH_2 [b]
15	0.08	0.07	0.01	0.29
16	0.80	–	0.12	0.06
17	1.00	–	0.33	0.02
27	–	0.02	0.08	0.02
28	–	0.07	0.06	0.08
29	–	0.14	0.34	0.03
30	–	0.02	–	0.02
31	–	–	–	0.03
42	–	0.22	0.02	0.25
43	–	1.00	0.11	0.50
44	–	0.02	0.25	0.66
45	–	–	1.00	0.04
59	–	–	–	1.00

Notes. [a]Fragmentation pattern from Bogan & Hand (1997), [b]Fragmentation pattern measured in this work.

Methylamine seen in TPD

The analysis of the mass fragmentation patterns of NH_2CHO, $OCN^-NH_4^+$ and CH_3CONH_2 is challenging due to their similar fragmentation patterns and proximity in desorption temperature (200-220 K). This point is emphasised in Table 7.3, which shows the fragmentation patterns of these molecules normalised to their main fragment for the most prominent masses. For example, the acetamide fragmentation pattern at m/z 44, 43 and 42 is difficult to match due to contributions of NH_2CHO and HNCO fragmentation channels. On the other hand it is also clear that these four species hardly contribute to fragment masses of m/z 30 and 31 (highlighted in red). The presence of these two masses as significant desorption features at ∼213 K is therefore peculiar (see top panel Fig. 7.7). In the experiment making use of $^{13}CH_4$ the same pattern is seen to shift to m/z 31 and 32 (see bottom panel Fig. 7.7).

This signal can not be explained as being a fragmentation channel of N-methylformamide. For one, the respective m/z 30/59 and m/z 31/60 ratios are ∼2.5 in both isotope experiments, which is much larger than the m/z 30/59 ratio of 0.6 of the pure N-methylformamide fragmentation pattern. Also, m/z 31 (or m/z 32 in the ^{13}C experiment) is not a prominent feature in the N-methylformamide fragmentation pattern (see Fig. 7.4). Another product must be responsible for these mass features and, within the constraints given by the experiment, this is likely methylamine (CH_3NH_2). A comparison between the m/z 31/30 (or 32/31) fragmentation channel (inset Fig. 7.7) shows that the experimental ratios match quite well with the given NIST value. The small deviations may be explained by minor contributions of fragmentation channels of HNCO and NH_2CHO to m/z 30 as can be distinguished with the $^{13}CH_4$:HNCO

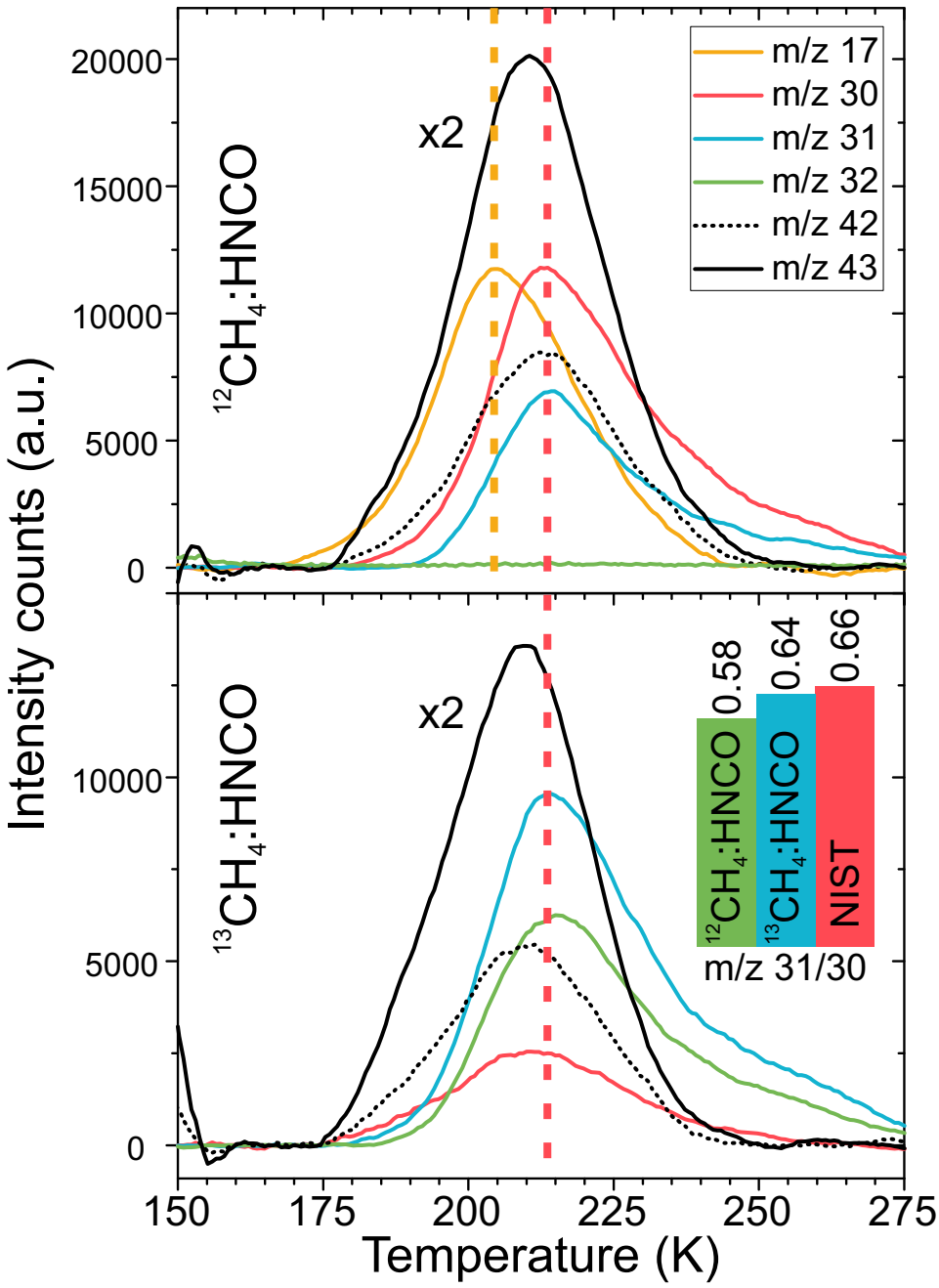

Figure 7.7: TPD trace of m/z 17 (yellow), 30 (red), 31 (blue), 32 (green), 42 (black dashed) and 43 (black, scalled by factor 1/2) of HNCO:$^{12}CH_4$ (experiment 1, top) and HNCO:$^{13}CH_4$ (experiment 3, bottom) ice. The dashed yellow line indicates the peak desorption temperature of m/z 17 and the red dashed line indicates the peak desorption temperature of m/z 30, 31 and 32. The inset gives the m/z 31/30 ratio for the two experiments and as given in the NIST database.

experiment. Comparisons of the m/z 29/30 and 28/30 ratios would help to further strengthen the identification of methylamine, however both HNCO and NH_2CHO have prominent fragmentation channels at these masses and therefore it is not possible to determine reliable ratios for these masses.

The peak desorption of m/z 30 and 31 occurs at 213 K, which is substantially higher than the desorption temperature of pure methylamine at 114 K (Theule et al. 2011). This is due to the formation of the $OCN^-CH_3NH_3^+$ salt complex. Just like ammonia, methylamine is a strong base and therefore readily engages in acid-base reactions with HNCO. Both $OCN^-NH_4^+$ and $OCN^-CH_3NH_3^+$ complexes are seen to decompose at different temperatures, as can be seen by the release of m/z 17 (ammonia) at 205 K and m/z 30 and 31 at 213 K, see Fig. 7.7. The desorption of HNCO around 215 K is therefore due to the decomposition of both salt complexes.

Secondary amides and larger species seen in TPD

The production of more complex species is also seen in these processed ices at a low level. Three features at m/z 73, 74 and 88 are detected in the TPD traces of CH_4:HNCO ice, see Fig. 7.8 (note the low signal count compared to Figs. 7.6 and 7.7). The first feature of m/z 73 at 218 K does not show up in the processed pure HNCO sample. In the mixture with $^{13}CH_4$ the feature shows up at m/z 75, indicating that two $^{13}C_x$ groups are part of this product. The m/z 74 feature at 258 K also does not show up in the pure HNCO processed ice and shifts by one mass to m/z 75 in the $^{13}CH_4$ mixture. Therefore this product incorporates only one $^{13}C_x$ group. m/z 88 is seen in all three the panels around 250 K. Since it is observed in the pure HNCO ice and no isotope shifts are seen, it must be a product of HNCO products or intermediates. Note that the low intensity signals limits the efficiency with which new products can be identified. For example, the middle panel of Fig. 7.8 seems to show a double peak which is not seen in the other two panels. This can hint to another product, but may also just be noise in the signal. Similarly, the bottom panel of Fig. 7.8 does a small feature at m/z 73, which can be a product that was not covered in the mass range of the top panel (experiment 1). For the moment, three relatively clear features of different products are seen, but potentially more complex products are present in these processed ices.

The secure identification of the three features is difficult because desorption temperatures are not available for candidate species and matching fragmentation patterns is hindered due to overlap with fragmentation channels of other species, mainly NH_2CHO, CH_3CONH_2 and NH_2CONH_2. Nevertheless, some candidates can be suggested, especially when one assumes that these higher mass species are derived from or related to the first generation of amides. For the m/z 73 signal propionamide ($CH_3CH_2CONH_2$), N-methylacetamide ($CH_3NHCOCH_3$) and dimethylformamide ($(CH_3)_2NCHO$) could be responsible. The latter two seem unlikely because they involve a CH_3-N bond, while the simplest of such species, N-methylformamide or CH_3NHCHO, was not detected as a product in these mixtures. The two most likely options for m/z 74 are methylurea ($CH_3NHCONH_2$) and 2-amino acetamide ($NH_2CH_2CONH_2$). Finally, for m/z = 88 two options are oxamide (NH_2-(CO)-(CO)-NH_2) or 1,2-hydrazinedicarboxaldehyde (CHO-NH-NH-CHO).

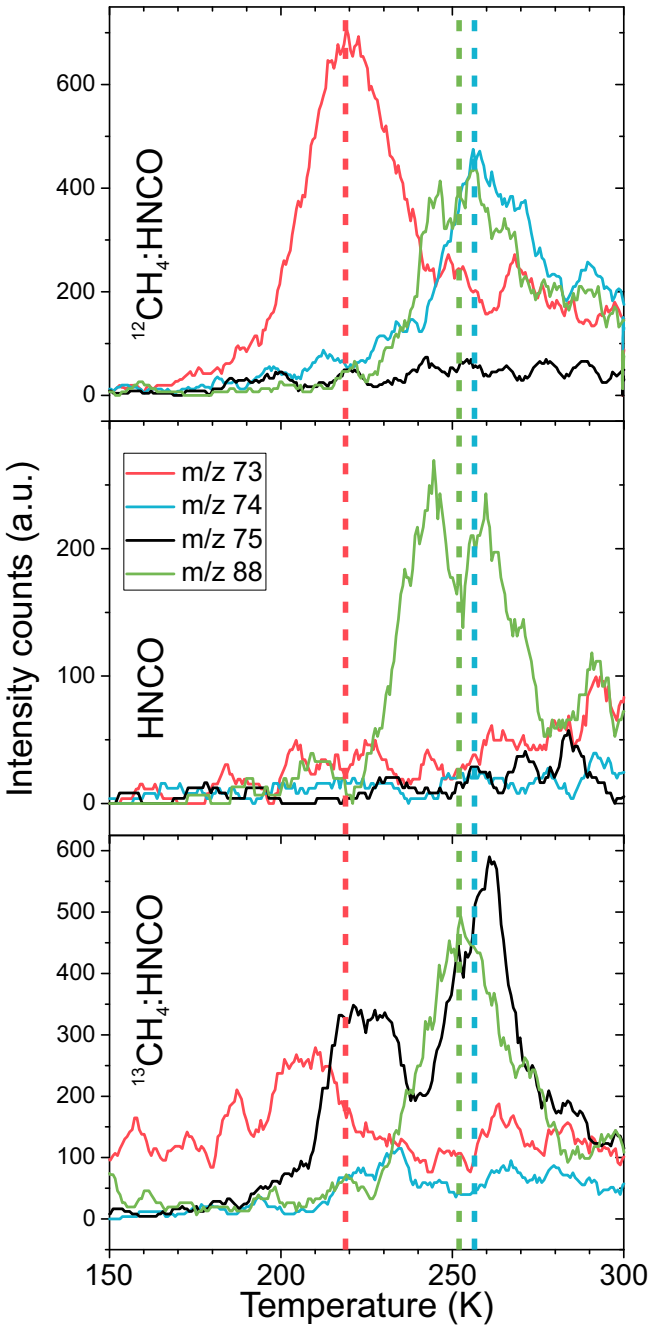

Figure 7.8: TPD of m/z 73 (red), 74 (blue), 75 (black) and 88 (green) between 150 and 300 K of VUV processed HNCO:$^{12}CH_4$ (top), HNCO (middle) and HNCO:$^{13}CH_4$ (bottom). Dashed lines indicate the desorption peaks of various products.

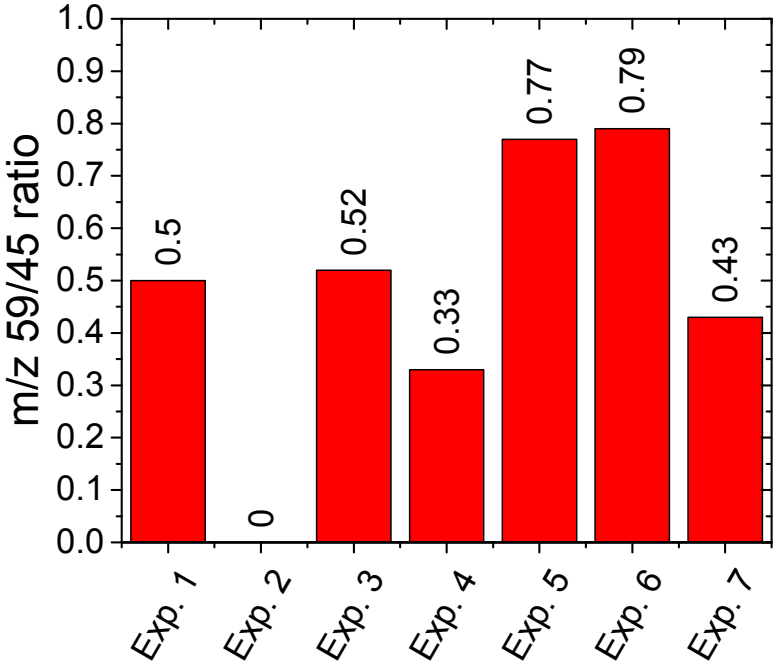

Figure 7.9: m/z 59 (acetamide) / 45 (formamide) ratio of the experiments performed in this work.

7.3.2. Comparison between experimental conditions

Besides the experiments presented above, additional experiments have been performed with different HNCO and methane abundances, lower Lyman-α intensities and dilution in a CO matrix to see how these parameters influence the production of acetamide. TPD data of formamide (m/z 45) and acetamide (m/z 59) are compared by determining the integrated area of each feature and deriving the m/z 59/45 ratio (see Fig. 7.9). Both NH_2CHO and CH_3CONH_2 are present in all experiments (except in pure HNCO, experiment 2), although absolute abundances do vary. A mass ratio of about 0.5 is found for experiment 1 and 3.

A first observation is that the m/z 59/45 ratio does not show any major shifts in ratio between the experiments and the deviation with respect to experiment 1 is at most $\pm$50%. This is despite processing by high fluence Lyman-α rich (Exp. 1-4) and low fluence Lyman-α poor (Exp. 5-7) radiation and high dilution in a CO matrix (6-7). This indicates that the processes that produce NH_2CHO and CH_3CONH_2 can occur in a variety of interstellar ices under different physical conditions.

Experiments 4 and 5 hint at a relationship with the CH_4 abundance. A low abundance (Exp. 4) results in less CH_3CONH_2 being produced, while a high abundance (Exp. 5) results in more produced CH_3CONH_2. The same effect is

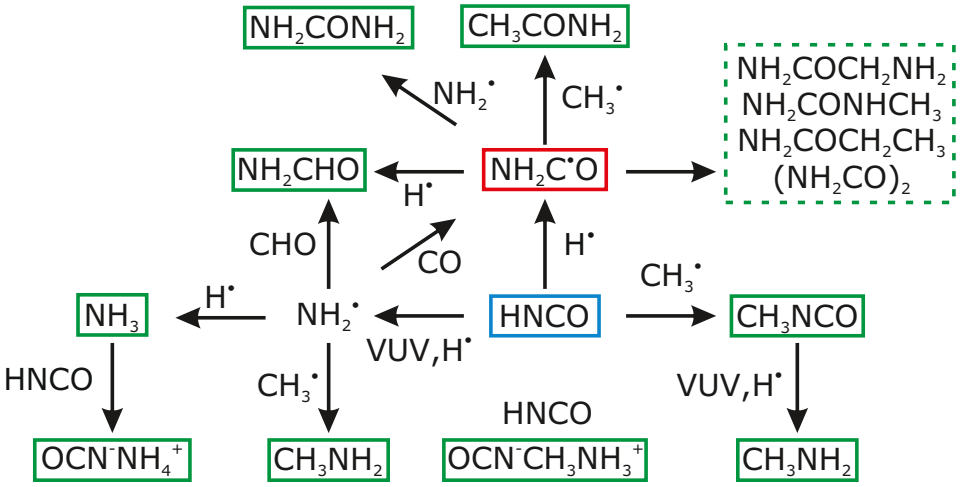

Figure 7.10: Possible reaction pathways to various amides and other products, constained by the findings of this work. Blue boxed is the parent species HNCO, green boxed are molecules detected in this work, green dashed boxes are suggested molecules that form. The important NH_2CO radical is shown in a red box, but not directly observed in the experiments.

not seen in experiments 6 and 7, which both have an equal HNCO to CH_4 ratio in the ice, albeit at different abundances. The CO matrix may be the cause of the observed difference in mass ratios.

In experiment 6 and 7 CH_4 and HNCO are relatively isolated in the CO matrix, with CH_4 to CO and HNCO to CO ratios of $\sim$1:10 and 1:30, respectively. Any molecular fragments produced from the VUV irradiation are expected to thermalised before reacting. This can hinder reactions of molecules, but still similar m/z 59/45 ratios with respect to the other experiments are found. This could hint to the production and storage of radicals in the ice. Upon heating the ice sample for the TPD, the radicals become mobile and produce the products that eventually are measured. This also makes it likely that NH_2CHO and CH_3CONH_2 have a common parent radical.

7.4. Discussion

7.4.1. Key reactions and reaction network

The results presented in Sec. 7.3 show that several complex, amide-bearing, molecules can be formed from VUV irradiated HNCO:CH_4 ices. Previous work by Ligterink et al. (2017) showed that CH_3NCO is formed in CH_4:HNCO mixed ices. In this work IR and QMS data show its presence as well. However, the related molecule CH_3NHCHO, suggested to form in hydrogen addition reactions, is not detected. This suggests that hydrogen addition reactions to CH_3NCO are not possible due to a high reaction barrier. Since hydrogen atoms in the CO matrix experiment are likely thermalised, it seems that both hot H-atom

addition and hydrogenation do not proceed. Alternatively, intermediates like $CH_3NHC^{\bullet}O$ or $CH_3N^{\bullet}CHO$ are not stable and efficiently destroyed, potentially under the influence of the VUV irradiation. CH_3NCO may be a source of the observed CH_3NH_2 via the reactions:

$$CH_3NCO + VUV \rightarrow CH_3N^{\bullet} + CO \tag{7.2}$$

$$CH_3NCO + H \rightarrow CH_3NHC^{\bullet}O \rightarrow CH_3N^{\bullet}H + CO \tag{7.3}$$

Hydrogenation and VUV irradiation experiments of pure CH_3NCO samples would help investigate these mechanisms and confirm or rule out the possibility to form N-methylformamide from methyl isocyanate. Besides forming CH_3NH_2 from CH_3NCO, other reaction pathways are possible as well. The VUV processing of the ice leads to various NH_x radicals and neutrals, as well as the NH_4^+ cation formed from HNCO. Reactions with CH_4, CH_3 and potentially smaller radicals derived from methane can occur and result in methylamine. Although in this work direct evidence for a specific formation mechanism of CH_3NH_2 is lacking, the main formation route described by Förstel et al. (2017) is plausible in this work as well:

$$^{\bullet}CH_3 +^{\bullet} NH_2 \rightarrow CH_3NH_2 \tag{7.4}$$

Two main scenarios can explain the formation of amides and their relation to each other. The first is hydrogen addition to HNCO which leads to the formation of the $NH_2C^{\bullet}O$ or carbamyl radical and is followed by radical recombination reactions. Hydrogen addition leading to the $N^{\bullet}CHO$ radical can be excluded due to the non-detection of CH_3NHCHO. All main products found in this work can be formed from $NH_2C^{\bullet}O$ in radical-radical addition reactions:

$$NH_2C^{\bullet}O + H^{\bullet} \rightarrow NH_2CHO \tag{7.5}$$

$$NH_2C^{\bullet}O +^{\bullet} NH_2 \rightarrow NH_2CONH_2 \tag{7.6}$$

$$NH_2C^{\bullet}O +^{\bullet} CH_3 \rightarrow CH_3CONH_2 \tag{7.7}$$

The second option starts with the dissociation of HNCO in NH and CO, followed by hydrogen addition reactions to form NH_2 and CHO. Formamide can be formed from the NH_2 + CHO reaction (Jones et al. 2011). However, the formation of CH_3CONH_2 and NH_2CONH_2 likely proceeds via the NH_2CO radical again formed from NH_2 + CO (see also Förstel et al. 2016, for this reaction). The experiments performed in a CO matrix likely have thermalised, cold or low energy hydrogen atoms in them. Since Noble et al. (2015) showed that (cold H-atom) hydrogenation of HNCO does not proceed, it strengthens the case that a radical recombination mechanism is responsible for the observed reaction products. However, with this mechanism one would intuitively also expect the formation of CH_3NHCHO. VUV irradiation experiments of NH_3:CO:CH_4 mixed ices should be conducted to further investigate this radical-radical recombination network.

If the $NH_2C^{\bullet}O$ radical indeed is a dominant radical in these ice mixtures, as above results suggest, desorption features found at m/z 73, 74 and 88 can be explained with it as well:

$$NH_2C^{\bullet}O +^{\bullet} CH_2CH_3 \rightarrow NH_2COCH_2CH_3 \tag{7.8}$$

$$NH_2C^{\bullet}O +^{\bullet} CH_2NH_2 \rightarrow NH_2COCH_2NH_2 \tag{7.9}$$

$$NH_2C^{\bullet}O +^{\bullet} NHCH_3 \rightarrow NH_2CONHCH_3 \tag{7.10}$$

$$NH_2C^{\bullet}O + NH_2C^{\bullet}O \rightarrow NH_2(CO)(CO)NH_2 \tag{7.11}$$

As above examples show, the $NH_2C^{\bullet}O$ radical can be an important intermediate for interstellar chemistry and the formation of complex amide-bearing molecules, as also indicated by Agarwal et al. (1985). In interstellar ices, its formation does not necessarily have to originate from HNCO or OCN^-, but can also be the result of NH_2 + CO addition or hydrogen abstraction of NH_2CHO.

The reactions described in this section result in the reaction network in Fig. 7.10. Starting from HNCO (blue blox), the NH_2CO radical (red box) can either directly or indirectly be formed. Subsequent reactions with H, CH_3 and NH_2 result in the formation of the primary amides (green boxes). Larger amides can be formed in similar reactions (dashed green box). Finally, the dissociation reactions are responsible for the formation of NH_3 and CH_3NH_2 and followed by acid-base reactions to form salts with HNCO.

7.4.2. Comparison with interstellar abundance ratios

It is possible to compare the experimental m/z 59/45 ratio of acetamide/formamide with interstellar abundances. If corrections are applied for the fragmentation pattern and the molecule specific electron impact absorption cross sections are taken into account, the experimental mass ratio can be converted into an abundance ratio (AR):

$$AR = \frac{C_{\text{formamide}}}{C_{\text{acetamide}}} \times \frac{F_{45,\text{formamide}}}{F_{59,\text{acetamide}}} \times \frac{I_{\text{acetamide}}}{I_{\text{formamide}}}, \tag{7.12}$$

where C_{species} is the total electron impact absorption cross section of the selected species at 70 eV ionization energy and F_{species} and I_{species} are the fragmentation ratio and the signal intensity, respectively, of a species at a certain mass. $I_{\text{acetamide}}/I_{\text{formamide}}$ is given by the m/z 59/45 ratio, and for the abundance comparison we take the ratio of 0.5 found in experiment 1. Fragmentation patterns give $F_{59,\text{acetamide}}$ = 0.29 and $F_{45,\text{formamide}}$ = 0.41. To our knowledge, total electron impact absorption cross sections have not experimentally been determined for these species. Theoretical predictions are available, however. The absorption cross section for formamide is given as 5.595 [2] (Gupta et al. 2014). A value for acetamide is not given, but for N-methylformamide it is calculated to be 10.063 [2]. We adopt this value with a generous error bar of ± 5 [2] for this comparison. From the given values an abundance ratio between acetamide and formamide of $0.4^{+0.39}_{-0.14}$ is derived.

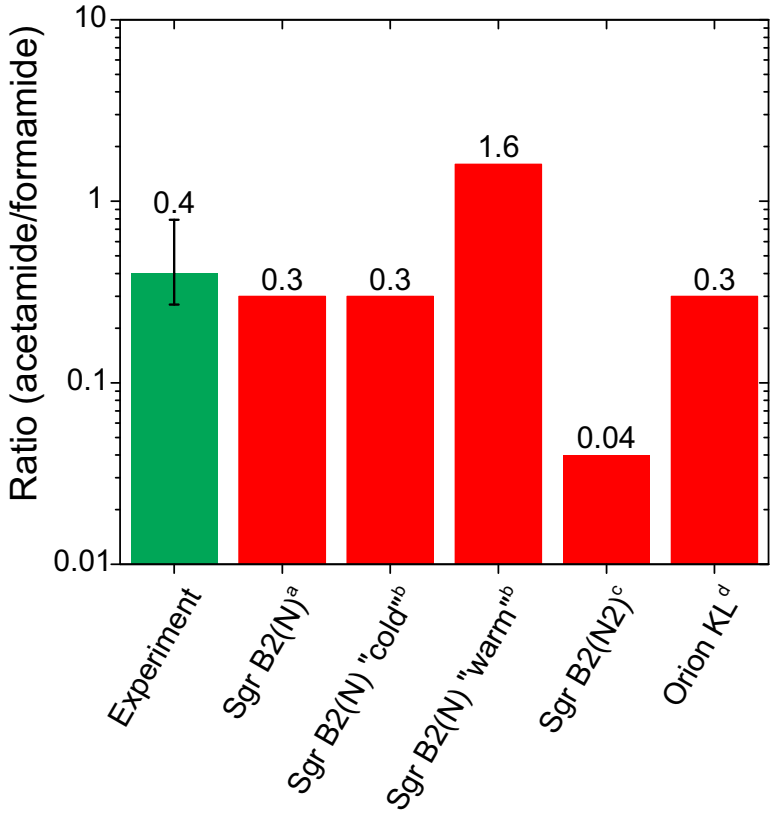

Figure 7.11: Acetamide over formamide abundance ratio as found in experiment 1 of this work compared with ratios derived in observational studies. [a]Hollis et al. (2006); [b]Halfen et al. (2011); [c]Belloche et al. (2017); [d]Cernicharo et al. (2016).

The experimental abundance ratio is compared with observationally determined ratios towards Sgr B2 and Orion KL in Fig. 7.11. In general, the experimental abundance ratio agrees well with observational abundance ratios. A clear outlier is the ratio of 0.04 derived by Belloche et al. (2017), in which interferometric data of ALMA are used to sample Sgr B2(N2). It contrast with the single dish observations toward Sgr B2(N) (Hollis et al. 2006; Halfen et al. 2011) but also with ALMA observations towards Orion KL (Cernicharo et al. 2016). The single dish observations sample larger spatial scales and cover emission from both Sgr B2(N1) and Sgr B2(N2), while Orion KL is not as extreme an environment as Sgr B2. These differences could explain the different abundance ratios found in these sources.

Overall the similarity between experimental and observational abundance ratios suggests that formamide and acetamide are related and both are formed in ice processes from a common parent molecule such as NH_2CO. More observations on the formamide and acetamide abundances towards other sources, particularly low-mass protostars, will aid in affirming this claim.

7.5. Conclusions

The main conclusions of this work are summarized as follows:

- The solid-state formation of acetamide (CH_3CONH_2) upon VUV irradiation is shown in CH_4:HNCO mixed ices, simultaneous with formamide (NH_2CHO) and urea (NH_2CONH_2), suggesting a common formational origin.
- Methyl isocyanate (CH_3NCO) is likely present in the ices studied, but formation of the related molecule N-methylformamide (CH_3NHCHO) is not seen, indicating that hydrogen addition to CH_3NCO is not possible or leads to the destruction of CH_3NCO.
- Formation of more complex molecules is seen, which could be species such as propanamide and methylcarbamide. These molecules can be targets to further investigate interstellar amide chemistry.
- Experimental evidence suggests that the NH_2CO radical is an important intermediate to the formation of acetamide and may also be an intermediate in the formation of formamide, urea and more complex species. In interstellar ice, the NH_2CO radical may also be formed from NH_2 + CO reactions or hydrogen abstraction of NH_2CHO.
- Comparison between the experimental and interstellar acetamide/formamide abundance ratios suggests that interstellar acetamide and formamide have a common formational origin that can be found in interstellar ice.